




Cite this: *Nanoscale*, 2022, **14**, 16065

Emerging laser-assisted vacuum processes for ultra-precision, high-yield manufacturing

Eunseung Hwang, ^{a,b} Joonmyung Choi ^{*a,b} and Sukjoon Hong ^{*a,b}

Laser technology is a cutting-edge process with a unique photothermal response, precise site selectivity, and remote controllability. Laser technology has recently emerged as a novel tool in the semiconductor, display, and thin film industries by providing additional capabilities to existing high-vacuum equipment. The *in situ* and *in operando* laser assistance enables using multiple process environments with a level of complexity unachievable with conventional vacuum equipment. This broadens the usable range of process parameters and directly improves material properties, product precision, and device performance. This review paper examines the recent research trends in laser-assisted vacuum processes (LAVPs) as a vital tool for innovation in next-generation manufacturing processing equipment and addresses the unique characteristics and mechanisms of lasers exclusively used in each study. All the findings suggest that the LAVP can lead to methodological breakthroughs in dry etching, 2D material synthesis, and chemical vapor deposition for optoelectronic devices.

Received 4th July 2022,
 Accepted 16th October 2022
 DOI: 10.1039/d2nr03649e
rsc.li/nanoscale

Introduction

Ultra-precise engineering of selected materials under a contamination-free environment has been crucial for creating modern electronics. To date, high-vacuum technology has responded well to industrial needs by developing appropriate equipment, often assisted by extreme processing conditions and specific chemicals introduced into the chamber.^{1–10} The raw material for the vacuum process, which is in the gaseous phase in general, is directly deposited on the substrate or utilized to etch the target bulk material, while the recent vacuum process enables atomic-scale processing and ensures wafer-scale productivity.^{11–19} As a result, the vacuum process has emerged as a core technology for the future advancement of electronic devices, covering additive and subtractive patterning capabilities with extremely high precision.

However, the state-of-the-art vacuum process faces several challenges regarding surface quality and process yield. The primary reason behind these challenges is that the process parameters (*e.g.*, pressure, temperature, and impinging chemical species) cannot be optimized over space and time. For example, although selective etching or mechanical reinforcement is achieved with specific chemical recipes and plasma

assistance, the vacuum process lacks site-selective operation in general usage since conventional vacuum technology is within a chamber under the same atmosphere.^{20–22} As a consequence, highly sophisticated equipment or the complex use of multiple chemicals in several steps has been inevitable to ensure spatial and temporal selectivity of the vacuum process. The introduction of additional experimental schemes and materials increases the overall process complexity and potentially interferes with the original system, adversely affecting the entire process.

The versatile advantages of a laser process are rediscovered to resolve these issues from the perspective of a supplementary process to the conventional vacuum process. The laser induces an entirely sterile and rapid photothermal reaction in designated areas, while the laser process can be readily integrated into the original system, showing that the laser-induced reactions occur remotely.^{23–25} Although the laser process itself cannot substitute the vacuum process, the laser-assisted strategies can improve conventional vacuum equipment rather significantly. It has been confirmed that the *in situ* and *in operando* assistance of a laser may bring versatile effects, such as selectively terminating competitive reactions, providing optimal processing conditions to the target substrate independent of the surroundings, or replacing the harmful chemicals.^{26,27} The latest results suggest that the laser is a tool compatible with the existing vacuum technology and a highly competitive supplementary process to substantially boost the performance of the advanced vacuum equipment independent from the existing approaches. To conclude, a laser can endow extra selectivity and compatibility to the vacuum equipment regardless of the addition of other strategies.

^aDepartment of Mechanical Design Engineering, Hanyang University, 222 Wangsimni-ro, Seongdong-gu, Seoul 04763, Republic of Korea.

E-mail: joonchoi@hanyang.ac.kr, sukjoonhong@hanyang.ac.kr

^bDepartment of Mechanical Engineering, BK21 FOUR ERICA-ACE Center, Hanyang University, 55 Hanyangdaehak-ro, Sangnok-gu, Ansan 15588, Republic of Korea

This minireview aims to report the latest advances in laser-assisted vacuum process (LAVP) for enhanced product quality and process yield as well as practical applications in the manufacturing industry. So far, there have been comprehensive review articles regarding the high-vacuum process, but LAVP was only introduced as a subset of conventional processes.^{28–31} Since the latest laser-assisted vacuum equipment is showing significant improvements from the conventional equipment, ensuring the high potential of LAVP for the next-generation manufacturing industry, we believe that it is timely to summarize the recent achievements of LAVP systematically and discuss the future development direction for further innovations in the vacuum process-based fabrication methods. We concentrate only on the LAVP reported in the past four years for a more focused review, while special attention has been paid to laser-assisted dry etching, synthesis, and chemical vapor deposition (CVD).

Laser-assisted dry etching

The high-resolution nanopatterning methods, such as focused electron-beam-induced etching (FEBIE) and focused ion-beam-induced etching (FIBIE), introduce a material removal process for the on-demand surface structure.^{32–34} A direct way to increase the etch rate in FEBIE is to maximize the source current for stimulating electron transport and reaction with precursors. However, the increased source current for a vigorous operation inevitably brings critical side effects. Due to the excessive reactions, the electrons of the by-products are redissociated into nonvolatile etch products (e.g., $\text{TiF}_4 + \text{e}^- \rightarrow \text{TiF}_3 + \text{F}$). The redissociation inhibits subsequent etching by forming a thin passivation layer.³⁵ The FIBIE faces similar challenges as it also deals with high levels of source current. The high dose of ions in FIBIE intensifies knock-on collisions and ion implantations, causing undesired subsurface damages during the etching process.^{36–38}

The *in situ* assistance of pulsed laser is one of the promising approaches for high-speed etching with minimal subsurface damages. The intermittent laser pulses instantaneously raise the surface temperature and facilitate the chemical reaction by elevating the desorption rates of precursors and by-products.³⁹ Noh *et al.* resolved the etch retardation of titanium (Ti) by laser-assisted focused electron-beam-induced etching (LAFEBIE) with XeF_2 precursor.⁴⁰ The photothermal heat expedites the insertion and desorption of volatile TiF_4 and delivers the precursor to the target region *via* localized surface diffusion. Similarly, Stanford *et al.* revealed the effect of laser chemical assistance with the aid of XeF_2 gas during the helium ion (He^+) milling of Ti thin film.⁴¹ The laser-assisted focused ion-beam-induced etching (LAFIBIE) method, synchronizing laser pulse with standard He^+ sputtering, improved the relative etch yield nine times and effectively mitigated the subsurface damages simultaneously. The experimental schematics and physical mechanics are explained in the previous literatures.^{40,41}

Zhang *et al.* reported a laser-assisted He^+ nanomachining of monolayer graphene without carbonaceous contamination to further improve the purity and surface quality after processing.⁴² The He^+ beam exposure breaks the adsorbed hydrocarbon species around the beam interaction region (Fig. 1a). Therefore, in the absence of an *in situ* laser assist, the deposition of carbon films suppresses the graphene etching. A study of different laser powers under constant He^+ beam exposure conditions suggests a competitive relationship between etching and deposition (Fig. 1b). The results verified that the photothermal desorption effectively suppresses the deposition of carbon placed under the steady-state condition and enables precise graphene milling.

Going one step further, anisotropic etching with a laser is also being attempted to completely alternate the energetic ion bombardment required when forming deep trench profiles. Peck *et al.* performed a 532 nm laser-assisted plasma etching (LAPE) on a Si wafer to demonstrate the polarization selectivity of lasers with wavelengths much larger than the feature size.⁴³ Simulation results of a 532 nm plane wave, exposed to the 22 nm half-pitch trench lines with an aspect ratio of 80, indicate that the Si trench structure behaves as a polarization-selective waveguide (Fig. 2a and b). The incident light polarized perpendicular to the trench profile propagates into the trench with a wavelength of about 370 nm, which lies between the vacuum wavelength ($\lambda_0 = 532$ nm) and the wavelength in Si ($n_{\text{Si},532 \text{ nm}} = 4.14$, $\lambda_{\text{Si},532 \text{ nm}} = 129$ nm), while the parallel light is mainly blocked at the surface.⁴⁴ The anisotropic etching properties predicted from wave optic simulations were also verified from experiments (Fig. 2c).

In summary, the laser local heating method is promising as a pioneering technology that can selectively terminate the competitive reaction between chemical substances in the graphene etching process. The optical polarization selectivity of

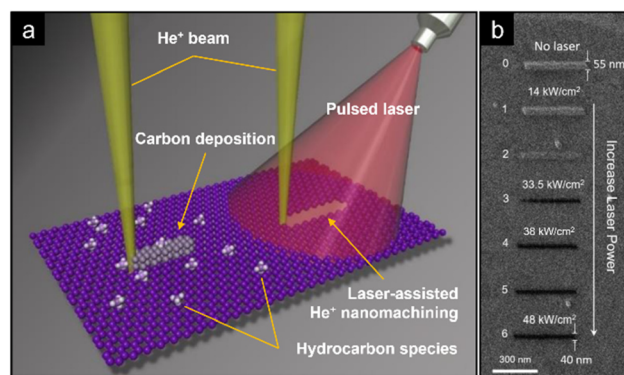


Fig. 1 (a) A schematic representation of He^+ beam exposure on a single layer graphene sample. The carbon contamination is restrained with the assistance of an *in situ* pulsed laser, and thus the He^+ milling is achieved. (b) A parametric study on the laser power with constant dosage (2×10^5 ions nm^{-1}) of He^+ beam scanning for 400 nm. The transition between the carbon deposition and He^+ milling of monolayer graphene is observed from the laser power over 33.5 kW cm^{-2} . This figure has been reproduced from ref. 42 with permission from MDPI, copyright 2019.

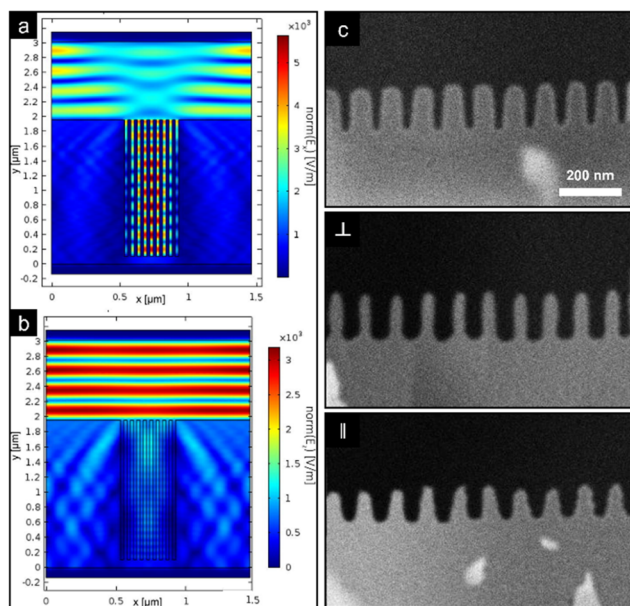


Fig. 2 Frequency domain simulations for 532 nm beam polarization under conditions (a) perpendicular and (b) parallel to the trench line. (c) Cross-sectional SEM images of the sample before etching and after LAPE was treated with perpendicular and parallel polarization. This figure has been reproduced from ref. 43 with permission from AIP Publishing, copyright 2018.

the laser is another essential feature that enables anisotropic etching without manipulating the source current. Therefore, the development of the laser-assisted etching processes has significantly contributed to the enhanced quality and yield of the product while successfully satisfying the demands for high-power operation.

Laser-assisted synthesis of 2D materials

2D materials are another promising candidate for innovative improvements through laser-assisted synthesis (LAS). Typically, 2D transition metal dichalcogenides (TMDCs) consist of three-atom thick materials with an MX_2 structure, where M is a transition metal (e.g., Mo, W, Re, and Nb.), and X is a chalcogen atom (e.g., S, Se, and Te).^{45,46} Strategies for synthesizing TMDCs are broadly classified into the following two categories: (i) the top-down method and (ii) the bottom-up method. The former is based on mechanical exfoliation, which has the advantage of being a low-cost and simple process but shows limited levels of thickness controllability, areal scalability, product quality, and process yield.^{47–49} Conversely, the latter is a method of growing gas-phase M^{n+} and $n\text{X}^{2-}$ on the substrate surface using CVD, metal-organic chemical vapor deposition (MOCVD), molecular beam epitaxy (MBE), pulsed laser deposition (PLD), *etc.*^{50–55} Particularly, the bottom-up scheme enables the creation of high-quality 2D single crystals and thin films because the mass flux can be managed low

enough to control the grains stacking over one another.^{49,56–58} One serious drawback is that rapid synthesis of the materials is difficult. The major obstacles are ambiguities in the selection, transport, and mixing of appropriate precursors, the need for an ultra-precise environment to control the complexity of chemical reaction pathways and growth kinetics, and the possibility of contamination by by-products.^{59,60} Among the conventional methods, direct laser vaporization of the TMDC surface through PLD provides a plausible solution to the contradiction arising from the difference between the evaporation and growth temperatures of 2D materials.^{53–55} However, considering the scale-up capability, the method is inappropriate for attaining large grains since the resultant thin films contain numerous grain boundaries.^{59,61}

Recently, a novel LAS technique has become a new approach to overcome the hurdles of current gas-phase growth systems. Monolayer 2D materials can be directly synthesized from bulk stoichiometric 2D powders using a strategy that decouples the evaporation from the growth process. Azam *et al.* demonstrated the potential of the LAS system by applying a continuous-wave (CW) CO_2 laser (10.6 μm wavelength) to the tube furnace through a zinc selenide (ZnSe) window (Fig. 3a).⁶² The laser heat is uniformly transferred to the TMDC powder through the graphite boat, producing a stoichiometric precursor vapor without disturbing the nucleation and growth environment (Fig. 3b).⁶³ Due to the high infrared absorbance of the graphite, the graphite boat heats up rapidly to each evaporation temperature of the four representative primary TMDCs 2D materials that are about 300 $^\circ\text{C}$ higher than the Si/SiO₂ substrate for growth (Fig. 3c). The quality of the grown crystals is assessed by atomic force microscopy (AFM), optical microscopic imaging, photoluminescence (PL) mapping, Raman spectroscopy, and transmission electron microscopy (TEM). The equivalent monolayer thickness is validated by the AFM height profile across the crystal boundary (Fig. 4a).^{64,65} Moreover, the strong PL emission mapping results along the shape of the crystals show the presence of a uniformly grown monolayer (Fig. 4b).^{45,48,66–68} The apparent peak of vibration mode (e.g., 242 cm^{-1} for MoSe_2) for out-of-plane motion and the absence of Raman peak associated with interlayer interactions (e.g., 353 cm^{-1} for MoSe_2) confirm the synthesized pristine single layer microstructure (Fig. 4c).^{68–70} The crystal structure of MoSe_2 , MoS_2 , WSe_2 , and WS_2 monolayers are further characterized in atomic resolution by annular dark-field scanning transmission electron microscopy (ADF-STEM) imaging *via* the image intensity contrast. The single-crystallinity and the hexagonal symmetry without any perceptible vacancies or defects are also recognized by the STEM and the fast Fourier transform (FFT) images (Fig. 4d).

The main advantage of LAS is that it can increase the purity and quality of the synthesized 2D materials while significantly reducing the complexity of the process. The LAS process does not require any hazardous gases except argon (Ar) for tuning the vapor flux in the chamber. Therefore, the kinetics involved in the existing bottom-up synthesis method can be simplified, and the growth rate of high-quality 2D materials can be accel-

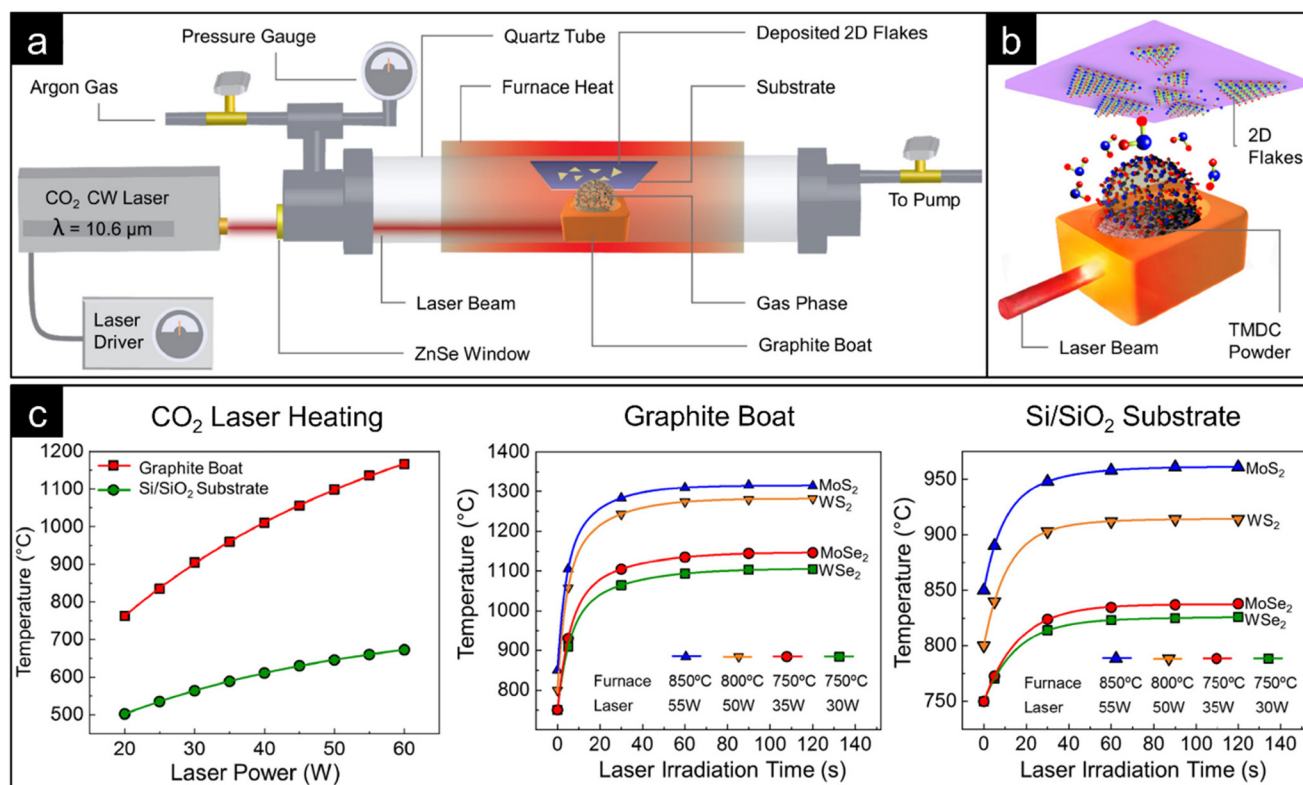


Fig. 3 (a) A scheme of LAS setup for 2D material synthesis. (b) A graphite boat containing the stoichiometric powders is laser heated to produce vaporization and subsequent growth of 2D flakes on a Si/SiO₂ substrate. (c) The temperature change profiles of the boat and the substrate during the LAS process for the growth of various 2D materials. At each operating condition, a significant temperature difference can be obtained between the graphite boat and the Si/SiO₂ substrate. This figure has been reproduced from ref. 62 with permission from IOP Publishing, copyright 2020.

erated. Table 1 summarizes the literature results showing the difference in size and quality of the synthesized 2D TMDCs materials depending on whether the LAS process is introduced. As explained in this section, the LAS process often shows superior performance compared to other methods in terms of material quality and process efficiency. When the CVD-based processes use molecular precursors together with additional chemical gases for an extended time to obtain microscale grains of moderate quality, the MBE utilizes elemental precursors without additional chemicals for high-purity synthesis. However, to enable rapid synthesis of high-purity 2D TMDCs materials, laser techniques, such as PLD and LAS, are introduced for direct stoichiometric transfer with minimal use of inert gas to set the chamber atmosphere. Moreover, the LAS holds a high potential for process scalability due to the uniform characteristics of sufficiently large grain sizes.

Laser-assisted chemical vapor deposition

Laser-assisted chemical vapor deposition (LACVD) has been extensively studied as an essential method in additive manufacturing.^{84,85} A representative and practical application technique of LACVD is the direct writing of graphene

materials. By adapting the hydrocarbons as a precursor, the programming of graphene patterning and the directional growth of carbon nanotubes are possible.^{86–88} This process is conducted in an environment where selective and rapid heating is achieved using lasers. Um *et al.* conducted direct writing of highly-ordered graphite thin films on a nickel foil by LACVD and transferred them to glass, demonstrating its potential for electronic applications.⁸⁹ Furthermore, Toh *et al.* reported the novel properties of centimeter-scale free-standing stable monolayer amorphous carbon (MAC) using LACVD.⁹⁰ Unlike conventional CVD-grown MAC at high temperature (>900 °C), a uniform MAC over several square centimeters was synthesized in less than 1 min at substrate temperatures as low as 200 °C.⁹¹ The distinguished mechanical properties of LACVD-grown MAC were verified by remaining stable for over a year under an ambient environment.

The laser irradiation process is expanding beyond being used as a simple heat source to the research that applies the optical and quantum mechanical properties of waves. One interesting optical property is the difference in energy density with wavelength. Fan *et al.* described the laser-induced vibrational excitations on a diamond deposition by using a wavelength-tunable CW CO₂ laser.⁹² As a result of irradiating a laser through the combustion CVD with tunable wavelength, it was found that the resonant mode of the ethylene (C₂H₄) mole-

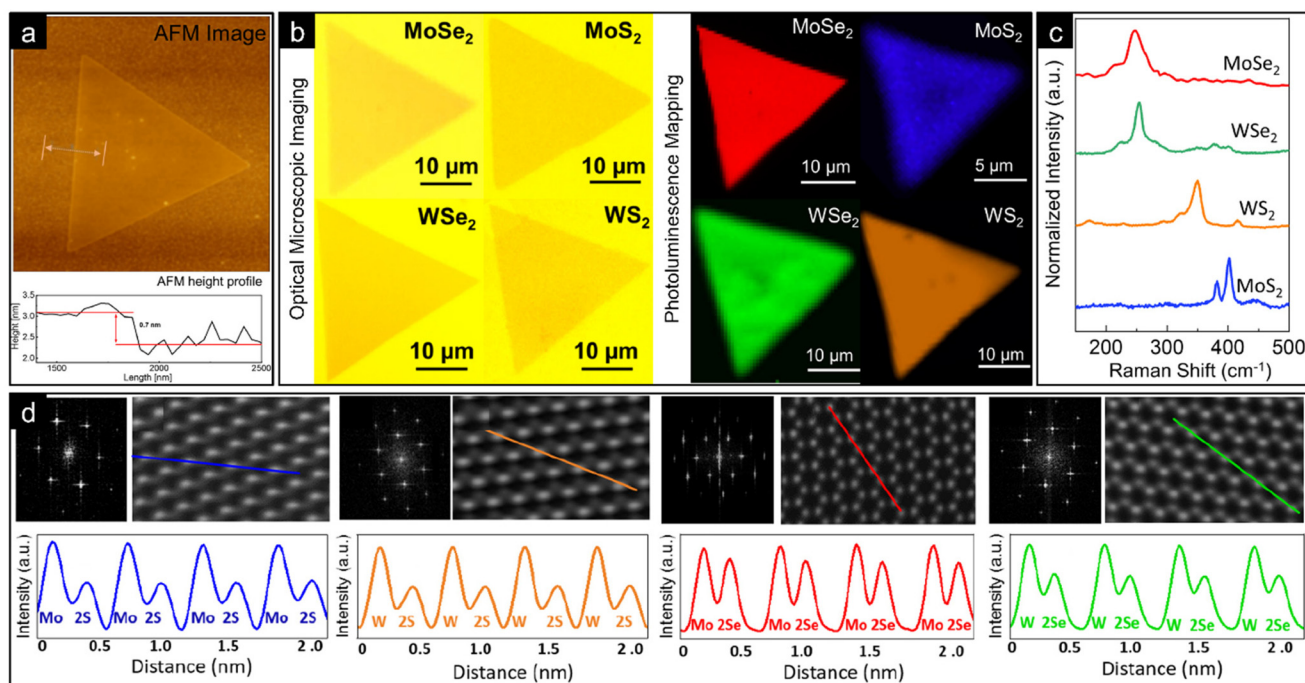


Fig. 4 Systematic analysis of the monolayer crystals synthesized. (a) An AFM image and the measured height profile across the crystal boundary. (b) A comparison between the optical images and the PL maps of each sample. (c) Raman spectra under 532 nm laser excitation source show the peak location of each material. (d) STEM and FFT images indicate the transition metal and chalcogen atoms, respectively. This figure has been reproduced from ref. 62 with permission from IOP Publishing, copyright 2020.

Table 1 Conventional 2D TMDCs synthesis methods

Methods	Precursors	Grain size	Thickness	Growth time	Purity	Ref.
CVD	Metal oxides and chalcogenides	Tens of microns	Mono to few-layer crystals	Minutes	Moderate	71–75
MOCVD	Metal-organic compounds	Few microns	Mono to few-layer crystals	Minutes to hours	Low	76–78
MBE	Elemental	Tens of nanometers	Mono to few-layer crystals	Hours	High	78–82
PLD	Stoichiometric target	Few to tens of nanometers	Mono to few-layer films	Seconds to minutes	High	53–55, 74 and 83
LAS	Stoichiometric powder	Tens of microns	Mono to few-layer crystals	Seconds to minutes	High	62

cule was 10.532 μm . This on-resonance excitation elevated the flame temperature, enhancing the deposition rate and diamond quality compared to the off-resonance excitations.

Meanwhile, in the case of a laser wavelength in the ultraviolet (UV) range, the high photon energy may lead to photodissociation of precursor molecules even at the lower fluences. Constantin *et al.* suggested the advantages of UV laser photolysis in diamond deposition by comparing 193 and 248 nm wavelengths.⁹³ The diamond deposition rate and quality are enhanced by photogenerated reactive species, such as OH, CH, and C₂ (Fig. 5a). Specifically, the three radicals act positively as carbon etchants (for OH), growth supplements (for CH), and crystal promoters (for C₂), respectively.^{94–98} What is important here is that the values of the increment rate of species peak intensity, growth rate, and quality factor at 193 nm outperform those of 248 nm despite the peak laser fluence of 900 mJ cm^{-2} , which is about 40 times lower (Fig. 5b). This is because an event occurs only when the quantized energy is sat-

isfied rather than when a large amount of energy is supplied.^{99–102} The photon energy of a 193 nm laser is higher than the C–H bonding energy of C₂H₂ and C₂H₄, which allows direct dissociation of hydrocarbon precursors, whereas a 248 nm laser has photon energy that only enables molecular excitation (Fig. 5c). The direct dissociation of the precursor has the effect of suppressing nondiamond carbon accumulation with a fast nucleation time. Accordingly, the nucleation time can be reduced as the fluence of the laser increases and the wavelength of the laser becomes shorter (Fig. 5d). This impedes the secondary nucleation from the pre-existing nuclei, preventing the original particle from stopping growth by multi-grain generation.¹⁰³ In conclusion, voluminous columnar diamond microcrystals can be obtained through UV laser-assisted combustion CVD (Fig. 5e).

Beyond the deposition of carbonaceous materials, studies of oxides or nitrides formation using LACVD have also provided interesting results.^{104–106} The diversification of depo-

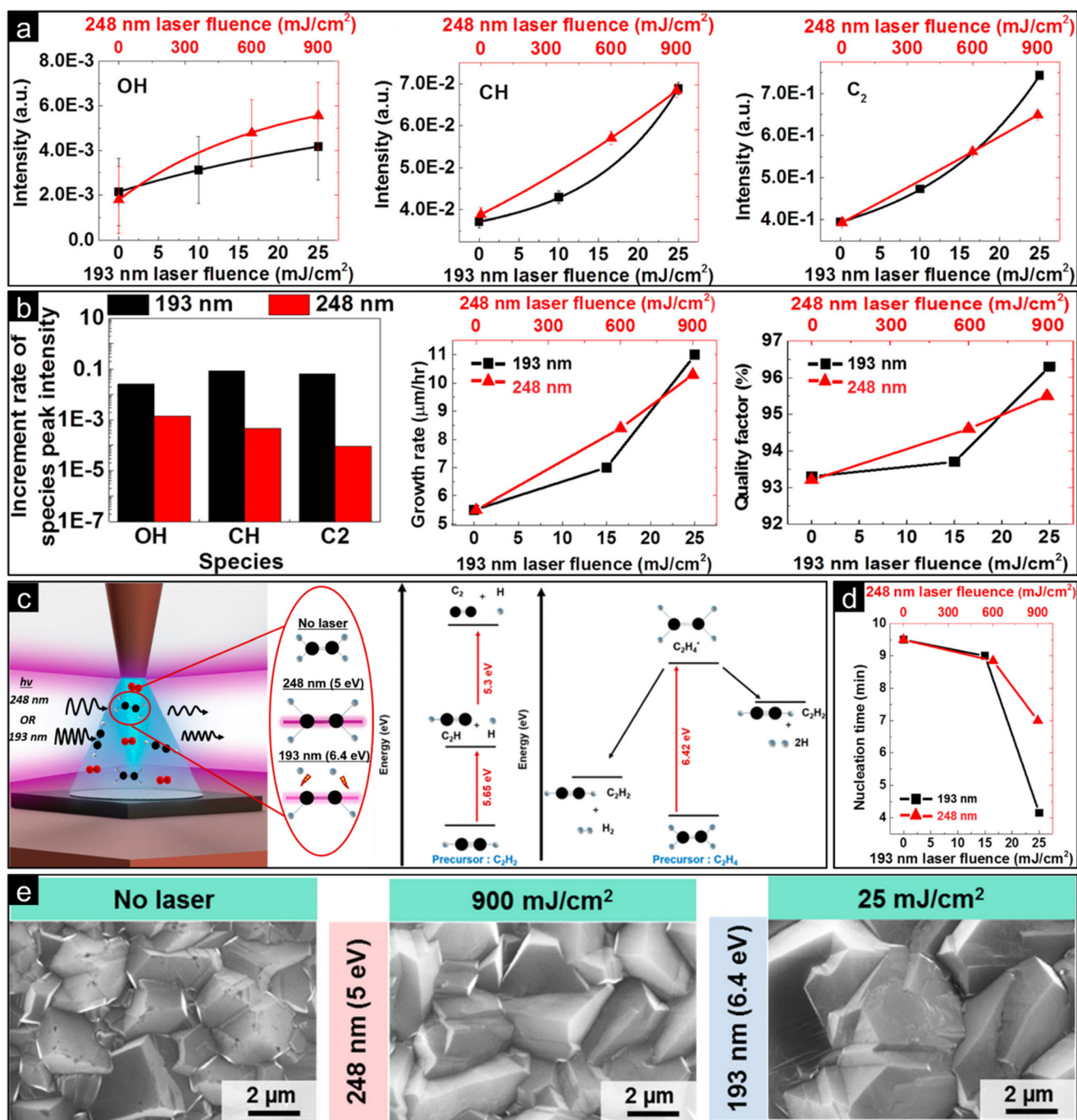


Fig. 5 (a) Integrated intensities of optical emission spectroscopy peaks assigned to each species (OH, CH, and C₂) with increasing laser fluences. (b) Comparative data of photogenerated species increment, diamond growth rate, and quality factor with 193 and 248 nm wavelengths. (c) A schematic of the UV laser-assisted combustion chemical vapor deposition and possible dissociation pathways of each precursor (C₂H₂ and C₂H₄). (d) Changes in nucleation time with laser fluence conditions at 193 and 248 nm wavelengths. (e) Optical microscopic images of deposited diamond films with or without the assistance of a UV laser. This figure has been reproduced from ref. 93 with permission from ACS Publications, copyright 2018.

sition materials marks the beginning of the next-generation manufacturing technology, as it can be directly utilized for several practical applications, especially in optoelectronics. For example, the rapid growth of high-quality gallium nitride (GaN) epilayers through LACVD allows a facile fabrication of GaN-based devices. The UV photodetectors, directly fabricated

by LACVD with a nine times faster growth rate, consist of smooth GaN layers and exhibit a high responsivity of 0.108 A W⁻¹ and a fast response time of 125 ns.¹⁰⁷ In other words, laser-assisted GaN devices with excellent optical properties can be fabricated using a simple and low-cost semiconductor deposition method.

Meanwhile, the stoichiometric deposition of silicon nitride is an important issue directly related to the process for encapsulation of organic light-emitting diodes (OLEDs) in the display industry.^{108–111} To date, plasma-enhanced chemical vapor deposition (PECVD) has been widely used in industry because of its high deposition rates at low processing temperatures, as well as good film uniformity over large substrate areas.^{112,113} However, the PECVD process does not entirely avoid the drawbacks, such as electrical damage to the device, mechanical deformation of the film, and nonstoichiometric silicon nitride film formation, significantly reducing the product yield.^{114–118} To overcome these limitations, An *et al.* suggested two-sequential processes comprising LACVD and laser-assisted plasma-enhanced chemical vapor deposition (LAPECVD) (Fig. 6a).¹¹⁹ By applying the 193 nm argon fluoride (ArF) pulsed laser, deficiencies, such as ion bombardment due to direct plasma exposure, residual stress formation in the deposited film, and low gas dissociation rate, are significantly resolved.¹²⁰ Particularly, the laser-assisted encapsulation processes present the most stable lifetime characteristics, which do not fall behind the glass encapsulation method (Fig. 6b). Kim *et al.* conducted a study directly comparing the character-

istics of silicon nitride deposited by LAPECVD and PECVD.¹²¹ The deposition rates of silicon nitride films by LAPECVD were higher than those of PECVD for all process conditions with varying plasma RF powers (Fig. 6c). As a result of optical emission spectroscopy (OES) analysis, it was confirmed that reactive gas dissociation was significantly improved in LAPECVD compared to PECVD.

There was also an advantage in terms of the physical and chemical properties of the deposited silicon nitride thin film. As the plasma RF power increases, the residual stress of the film decreased to 147 MPa, which is 34% lower than the film deposited with PECVD (Fig. 6d). The X-ray photoelectron spectroscopy (XPS) results suggest that the origin of the low residual stress is due to the improved chemical composition; narrow XPS scan data of Si 2p and N 1s close to stoichiometric silicon nitride (Si_3N_4) are secured by LAPECVD (Fig. 6e). The enhanced chemical robustness also affects the selectivity of dry etching under a CF_4/O_2 plasma (Fig. 6f). Silicon nitride deposited by LAPECVD can form denser structures with higher nitridation, which leads to lower etch rates.¹²²

The integrity of the organic layer was evaluated by measuring the electrical damage that occurred to the substrate during

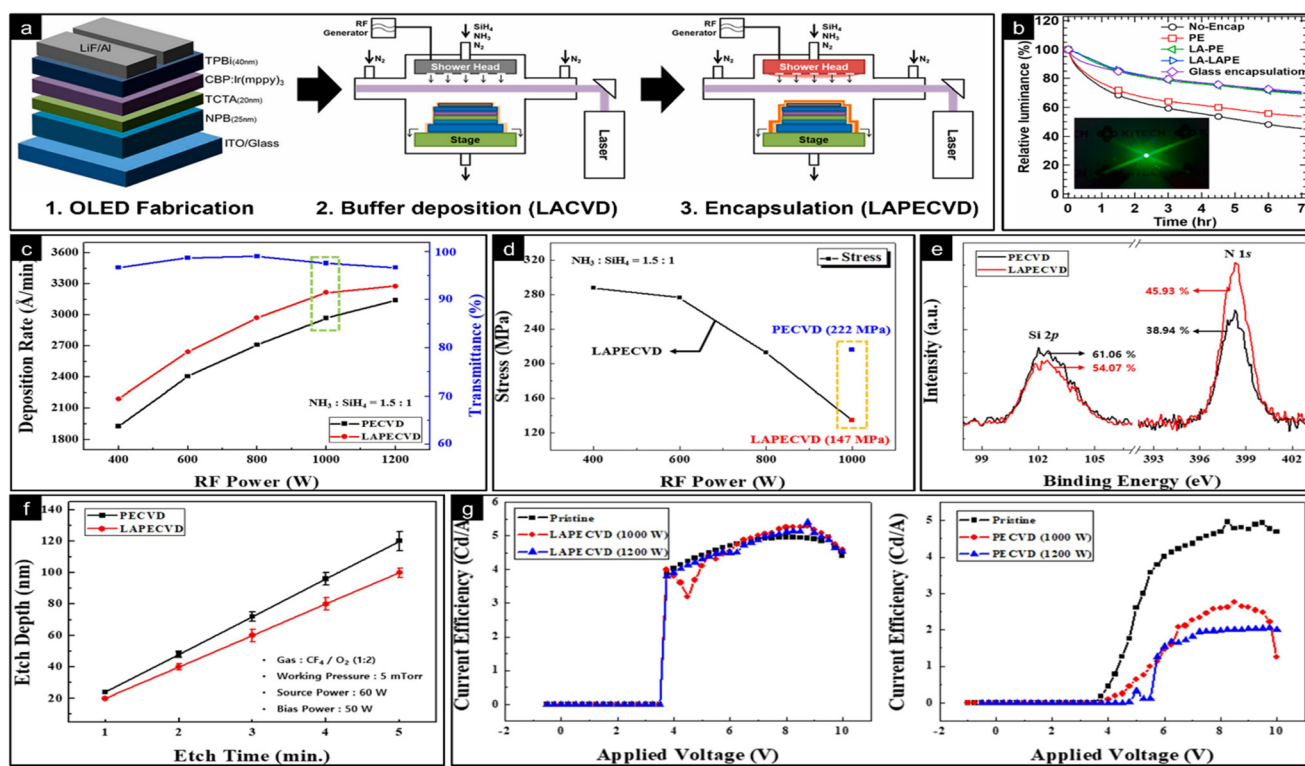


Fig. 6 (a) Schematics of the fabrication process for silicon nitride encapsulation using LACVD and LAPECVD. (b) Electroluminescence lifetime characteristics of OLEDs by different encapsulation layers (PE: PECVD only, LA-PE: PECVD after LACVD, LA-LAPE: LAPECVD after LACVD) under constant luminance of 5000 cd m^{-2} . (Inset: a luminescence image of the OLEDs under 7 V bias.) (c) Deposition rates of silicon nitride for PECVD and LAPECVD with a fixed ArF laser power density of 75 mW mm^{-2} and the optical transmittance of silicon nitride thin films. (d) Residual stress of silicon nitride films with the functions of plasma RF power. (e) XPS narrow scan data of Si 2p (102 eV) and N 1s (398 eV) with each atomic percentage. (f) Dry etch characteristics using a gas mixture of CF_4 and O_2 (1:2) and working pressure of 5 mTorr. (g) Electrical damage evaluation of OLEDs after the passivation process by silicon nitride deposition using LAPECVD and PECVD operated for 1 min. This figure has been reproduced from ref. 119 and 121 with permission from Elsevier, copyright 2021.

the process. The current efficiency is derived from the measurement, and it becomes a practical evaluation method directly related to the overall performance of the OLED device.^{122–126} As a result, the current efficiency of the LAPECVD method maintained the pristine level of luminance, while significant degradation was observed with the PECVD method (Fig. 6g). Therefore, by applying the LACVD-LAPECVD two-step process, silicon nitride can be deposited in the lower region only with the ArF laser before encapsulation. The deposited layer acts as a buffer for post-processing to prevent electrical damage from occurring in the plasma environment.

Recent studies on LACVD are exploring how to apply laser devices to enhance the practical quality and yield of products. By adding the extremely high but site-selective energy supply process through laser irradiation into the existing vacuum equipment, the molecules participating in the reaction can be efficiently decomposed, saving energy consumption effectively. In addition, the above-mentioned method of encapsulating OLEDs with silicon nitrides through LACVD-LAPECVD improves coating stability and thus can directly contribute to increasing product yield in the display industry. In summary, the improvement effect of the vacuum equipment performance by the laser-assisted process is evident and has high potential. Theoretical studies to elucidate unexplored mechanisms and engineering considerations to optimize processes are required in the near future.

Summary and outlook

The present review has compiled the possibility of material processing, synthesis, and deposition improvement through laser assistance to the latest vacuum equipment technology. In all the processes mentioned, the unique thermal and optical properties of the laser were actively utilized, and it was confirmed that there were substantial improvements in processing quality level and product yield. The contributions and achievements of laser equipment in each high vacuum process covered so far are summarized below.

Dry etching

Local heating by *in situ* laser irradiation effectively prevents the build-up of by-products over the process area. One of the significant problems that can happen during the FEBIE and FIBIE processes is etching retardation, as explained in the previous section, which is the phenomenon found in the volatile etch products becoming nonvolatile due to electron redissociation. The laser-assisted method can avoid such etching retardation that occurs primarily under excessive source current conditions. The optical polarization selectivity of the laser offers another potential scalability for laser-assisted dry etching. The anisotropic dry etching requires much effort in the careful design of the mask to protect the sidewalls of a cavity during ion bombardment while maintaining the high aspect ratio trenches. Therefore, laser assistance can be a complete alternative to a high-power operation in dry etching.

Synthesis of (2D) nanomaterials

Obtaining high-quality single crystals with satisfactory yields on the nanoscale is a challenging task in vacuum science and technology. The controllability and productivity of nanomaterial synthesis always conflict with each other under the set process conditions of the equipment, which significantly reduces the industrial value. The laser-assisted synthesis method overcomes this paradox by applying different temperatures through selective laser irradiation to the source and substrate in one process environment. Therefore, optimized growth conditions can be achieved to produce stoichiometric and highly crystalline nanofilms. Both synthesis rate and purity are improved without significantly increasing the overall steps except for the laser irradiation process. The absence of hazardous chemicals in the process is another advantage.

Coating

The effectiveness of laser assistance in the deposition process of various materials, including graphene, diamond, oxides, and nitrides, has been validated several times. The rapid and selective heating performance of lasers, discussed earlier, is the main driving force behind the improvement of the deposition process. In addition, the optical properties according to the wavelength of the laser further broaden the basis for exploring the optimal deposition process conditions for each material. This enables the formation of coated films with high levels of mechanical, chemical, and electrical properties that have not been previously reported. Therefore, there is a possibility of suggesting a new paradigm for the display industry (e.g., OLED encapsulation processes), which has been considered close to technological saturation.

Our investigation of the relevant research in the last four years tells us that laser processes hold high potential to push the boundary of the existing concepts or to accept new materials, e.g., 2D materials, for ground-breaking devices at a minimized invasion of the existing high-vacuum technology. Recent developments and advances in new laser sources, such as organic solid-state lasers, will also be highly synergistic.¹²⁷ By offering various aspects of spectral and chemical tunability, such as low refractive indexes, mechanical flexibilities, and low thresholds, it is expected that the diversification and complexity of laser integration technology will become possible in a broader range. As a concluding remark, we would like to emphasize again that improvements in the vacuum process are an urgent matter since the semiconductor shortage has been continued for an extended period. However, it should also be noted that adding laser irradiation processes to the vacuum equipment is accompanied by temporary risks and, therefore, may not be compatible with the leading-edge industries under active development and optimization. In these regards, we expect that the laser-assisted vacuum process can be relatively more valuable for trailing-edge semiconductor industries, which still account for a large portion of the total revenue but requires a significant upsurge in its throughput without the compensation of the product quality.

Author contributions

E. H. conceived the idea and wrote the original draft with the reproduction of figures. J. C. developed the concept. J. C. and S. H. revised the manuscript and supervised the overall project.

Conflicts of interest

There are no conflicts to declare.

Acknowledgements

This work was supported by the Basic Research Program through the National Research Foundation of Korea (NRF) (No. 2022R1C1C1006593 & 2022R1F1A1063199). Moreover, this work was supported by the Institute of Information & Communications Technology Planning & Evaluation (IITP) grant funded by the Korean government MSIT (No. 2022-0-00059, Development of an automated parcel unloading system using a mobile manipulator and AI-based object recognition technology). This work was supported by the Korea Evaluation Institute of Industrial Technology (KEIT) grant funded by the Korean government (MOTIE) (No. 20019223, Developing Automated Defect Repair AFM System with Detecting and Analyzing Defect of EUV Mask). E. H. acknowledges a fellowship from the Hyundai Motor Chung Mong-Koo Foundation.

References

- 1 S. Barja, S. Refaely-Abramson, B. Schuler, D. Y. Qiu, A. Pulkin, S. Wickenburg, H. Ryu, M. M. Ugeda, C. Kastl, C. Chen, C. Hwang, A. Schwartzberg, S. Aloni, S.-K. Mo, D. Frank Ogletree, M. F. Crommie, O. V. Yazyev, S. G. Louie, J. B. Neaton and A. Weber-Bargioni, *Nat. Commun.*, 2019, **10**, 3382.
- 2 G.-L. Xu, Q. Liu, K. K. S. Lau, Y. Liu, X. Liu, H. Gao, X. Zhou, M. Zhuang, Y. Ren, J. Li, M. Shao, M. Ouyang, F. Pan, Z. Chen, K. Amine and G. Chen, *Nat. Energy*, 2019, **4**, 484–494.
- 3 G. Yuan, D. Lin, Y. Wang, X. Huang, W. Chen, X. Xie, J. Zong, Q.-Q. Yuan, H. Zheng, D. Wang, J. Xu, S.-C. Li, Y. Zhang, J. Sun, X. Xi and L. Gao, *Nature*, 2020, **577**, 204–208.
- 4 Y.-L. Hong, Z. Liu, L. Wang, T. Zhou, W. Ma, C. Xu, S. Feng, L. Chen, M.-L. Chen, D.-M. Sun, X.-Q. Chen, H.-M. Cheng and W. Ren, *Science*, 2020, **369**, 670–674.
- 5 H. Lu, Y. Liu, P. Ahlawat, A. Mishra, W. R. Tress, F. T. Eickemeyer, Y. Yang, F. Fu, Z. Wang, C. E. Avalos, B. I. Carlsen, A. Agarwalla, X. Zhang, X. Li, Y. Zhan, S. M. Zakeeruddin, L. Emsley, U. Rothlisberger, L. Zheng, A. Hagfeldt and M. Grätzel, *Science*, 2020, **370**, eabb8985.
- 6 C. Lu, Z. Sun, L. Yu, X. Lian, Y. Yi, J. Li, Z. Liu, S. Dou and J. Sun, *Adv. Energy Mater.*, 2020, **10**, 2001161.
- 7 C. Li, Z. Sun, T. Yang, L. Yu, N. Wei, Z. Tian, J. Cai, J. Lv, Y. Shao, M. H. Rummeli, J. Sun and Z. Liu, *Adv. Mater.*, 2020, **32**, 2003425.
- 8 M. Wang, M. Huang, D. Luo, Y. Li, M. Choe, W. K. Seong, M. Kim, S. Jin, M. Wang, S. Chatterjee, Y. Kwon, Z. Lee and R. S. Ruoff, *Nature*, 2021, **596**, 519–524.
- 9 L. Jiao, J. Li, L. L. Richard, Q. Sun, T. Stracensky, E. Liu, M. T. Sougrati, Z. Zhao, F. Yang, S. Zhong, H. Xu, S. Mukerjee, Y. Huang, D. A. Cullen, J. H. Park, M. Ferrandon, D. J. Myers, F. Jaouen and Q. Jia, *Nat. Mater.*, 2021, **20**, 1385–1391.
- 10 J. A. Zamora Zeledón, M. B. Stevens, G. T. K. K. Gunasooriya, A. Gallo, A. T. Landers, M. E. Kreider, C. Hahn, J. K. Nørskov and T. F. Jaramillo, *Nat. Commun.*, 2021, **12**, 620.
- 11 L. Zhang, R. Si, H. Liu, N. Chen, Q. Wang, K. Adair, Z. Wang, J. Chen, Z. Song, J. Li, M. N. Banis, R. Li, T.-K. Sham, M. Gu, L.-M. Liu, G. A. Botton and X. Sun, *Nat. Commun.*, 2019, **10**, 4936.
- 12 Q. Wang, Y. Lei, Y. Wang, Y. Liu, C. Song, J. Zeng, Y. Song, X. Duan, D. Wang and Y. Li, *Energy Environ. Sci.*, 2020, **13**, 1593–1616.
- 13 S. S. Cheema, D. Kwon, N. Shanker, R. dos Reis, S.-L. Hsu, J. Xiao, H. Zhang, R. Wagner, A. Datar, M. R. McCarter, C. R. Serrao, A. K. Yadav, G. Karbasian, C.-H. Hsu, A. J. Tan, L.-C. Wang, V. Thakare, X. Zhang, A. Mehta, E. Karapetrova, R. V. Chopdekar, P. Shafer, E. Arenholz, C. Hu, R. Proksch, R. Ramesh, J. Ciston and S. Salahuddin, *Nature*, 2020, **580**, 478–482.
- 14 H. Yan, K. He, I. A. Samek, D. Jing, M. G. Nanda, P. C. Stair and J. M. Notestein, *Science*, 2021, **371**, 1257–1260.
- 15 D. X. Luong, K. V. Bets, W. A. Algozeeb, M. G. Stanford, C. Kittrell, W. Chen, R. V. Salvatierra, M. Ren, E. A. McHugh, P. A. Advincula, Z. Wang, M. Bhatt, H. Guo, V. Mancevski, R. Shahsavari, B. I. Yakobson and J. M. Tour, *Nature*, 2020, **577**, 647–651.
- 16 S. Chen, M. R. Mahmoodi, Y. Shi, C. Mahata, B. Yuan, X. Liang, C. Wen, F. Hui, D. Akinwande, D. B. Strukov and M. Lanza, *Nat. Electron.*, 2020, **3**, 638–645.
- 17 N. Li, Q. Wang, C. Shen, Z. Wei, H. Yu, J. Zhao, X. Lu, G. Wang, C. He, L. Xie, J. Zhu, L. Du, R. Yang, D. Shi and G. Zhang, *Nat. Electron.*, 2020, **3**, 711–717.
- 18 M. Chubarov, T. H. Choudhury, D. R. Hickey, S. Bachu, T. Zhang, A. Sebastian, A. Bansal, H. Zhu, N. Trainor, S. Das, M. Terrones, N. Alem and J. M. Redwing, *ACS Nano*, 2021, **15**, 2532–2541.
- 19 M. A. Giambra, V. Mišeikis, S. Pezzini, S. Marconi, A. Montanaro, F. Fabbri, V. Sorianello, A. C. Ferrari, C. Coletti and M. Romagnoli, *ACS Nano*, 2021, **15**, 3171–3187.
- 20 Y.-H. Tsai and M. Wang, *J. Vac. Sci. Technol., B: Nanotechnol. Microelectron.: Mater., Process., Meas., Phenom.*, 2022, **40**, 013201.
- 21 Z. J. Han, A. T. Murdock, D. H. Seo and A. Bendavid, *2D Mater.*, 2018, **5**, 032002.

- 22 A. S. Grenadyorov, A. A. Solovyev, K. V. Oskomov and V. S. Sypchenko, *Surf. Coat. Technol.*, 2018, **349**, 547–555.
- 23 D. Bäuerle, *Laser processing and chemistry*, Springer Science & Business Media, 2013.
- 24 Y. Fujiwara, K. Maehashi, Y. Ohno, K. Inoue and K. Matsumoto, *Jpn. J. Appl. Phys.*, 2005, **44**, 1581.
- 25 D. J. Hwang, S.-G. Ryu and C. P. Grigoropoulos, *Nanotechnology*, 2011, **22**, 385303.
- 26 B. Y. Chang, S. Shin, J. Santamaria and I. R. Sola, *Chem. Phys.*, 2014, **442**, 18–25.
- 27 M. K. Das, J. A. Bobb, A. A. Ibrahim, A. Lin, K. M. AbouZeid and M. S. El-Shall, *ACS Appl. Mater. Interfaces*, 2020, **12**, 23844–23852.
- 28 V. M. Donnelly and A. Kornblit, *J. Vac. Sci. Technol., A*, 2013, **31**, 050825.
- 29 Y. Yan, J. Miao, Z. Yang, F.-X. Xiao, H. B. Yang, B. Liu and Y. Yang, *Chem. Soc. Rev.*, 2015, **44**, 3295–3346.
- 30 S. Hong, H. Lee, J. Yeo and S. H. Ko, *Nano Today*, 2016, **11**, 547–564.
- 31 C. Backes, A. M. Abdelkader, C. Alonso, A. Andrieux-Ledier, R. Arenal, J. Azpeitia, N. Balakrishnan, L. Banszerus, J. Barjon and R. Bartali, *2D Mater.*, 2020, **7**, 022001.
- 32 A. Ganczarczyk, M. Geller and A. Lorke, *Nanotechnology*, 2010, **22**, 045301.
- 33 D. S. Fox, P. Maguire, Y. Zhou, C. Rodenburg, A. O'Neill, J. N. Coleman and H. Zhang, *Nanotechnology*, 2016, **27**, 195302.
- 34 V. Dergianlis, M. Geller, D. Oing, N. Wöhrle and A. Lorke, *Nanotechnology*, 2019, **30**, 365302.
- 35 M. G. Lassiter and P. D. Rack, *Nanotechnology*, 2008, **19**, 455306.
- 36 R. Livengood, S. Tan, Y. Greenzweig, J. Notte and S. McVey, *J. Vac. Sci. Technol., B: Microelectron. Nanometer Struct.–Process., Meas., Phenom.*, 2009, **27**, 3244–3249.
- 37 Y. Drezner, Y. Greenzweig, D. Fishman, E. van Veldhoven, D. J. Maas, A. Raveh and R. H. Livengood, *J. Vac. Sci. Technol., B: Nanotechnol. Microelectron.: Mater., Process., Meas., Phenom.*, 2012, **30**, 041210.
- 38 K. Kohama, T. Iijima, M. Hayashida and S. Ogawa, *J. Vac. Sci. Technol., B: Nanotechnol. Microelectron.: Mater., Process., Meas., Phenom.*, 2013, **31**, 031802.
- 39 N. A. Roberts, C. M. Gonzalez, J. D. Fowlkes and P. D. Rack, *Nanotechnology*, 2013, **24**, 415301.
- 40 J. Noh, J. Fowlkes, R. Timilsina, M. Stanford, B. Lewis and P. Rack, *ACS Appl. Mater. Interfaces*, 2015, **7**, 4179–4184.
- 41 M. G. Stanford, K. Mahady, B. B. Lewis, J. D. Fowlkes, S. Tan, R. Livengood, G. A. Magel, T. M. Moore and P. D. Rack, *ACS Appl. Mater. Interfaces*, 2016, **8**, 29155–29162.
- 42 C. Zhang, O. Dyck, D. A. Garfinkel, M. G. Stanford, A. A. Belianinov, J. D. Fowlkes, S. Jesse and P. D. Rack, *Nanomaterials*, 2019, **9**, 1394.
- 43 J. A. Peck and D. N. Ruzic, *J. Vac. Sci. Technol., A*, 2018, **36**, 021301.
- 44 G. E. Jellison, F. A. Modine, C. W. White, R. F. Wood and R. T. Young, *Phys. Rev. Lett.*, 1981, **46**, 1414–1417.
- 45 X. Song, J. Hu and H. Zeng, *J. Mater. Chem. C*, 2013, **1**, 2952–2969.
- 46 J. Zhou, J. Lin, X. Huang, Y. Zhou, Y. Chen, J. Xia, H. Wang, Y. Xie, H. Yu, J. Lei, D. Wu, F. Liu, Q. Fu, Q. Zeng, C.-H. Hsu, C. Yang, L. Lu, T. Yu, Z. Shen, H. Lin, B. I. Yakobson, Q. Liu, K. Suenaga, G. Liu and Z. Liu, *Nature*, 2018, **556**, 355–359.
- 47 K. S. Novoselov, D. Jiang, F. Schedin, T. J. Booth, V. V. Khotkevich, S. V. Morozov and A. K. Geim, *Proc. Natl. Acad. Sci. U. S. A.*, 2005, **102**, 10451–10453.
- 48 K. F. Mak, C. Lee, J. Hone, J. Shan and T. F. Heinz, *Phys. Rev. Lett.*, 2010, **105**, 136805.
- 49 J. R. Brent, N. Savjani and P. O'Brien, *Prog. Mater. Sci.*, 2017, **89**, 411–478.
- 50 J. Yu, J. Li, W. Zhang and H. Chang, *Chem. Sci.*, 2015, **6**, 6705–6716.
- 51 S. Cwik, D. Mitoraj, O. Mendoza Reyes, D. Rogalla, D. Peeters, J. Kim, H. M. Schütz, C. Bock, R. Beranek and A. Devi, *Adv. Mater. Interfaces*, 2018, **5**, 1800140.
- 52 D. Fu, X. Zhao, Y.-Y. Zhang, L. Li, H. Xu, A. R. Jang, S. I. Yoon, P. Song, S. M. Poh, T. Ren, Z. Ding, W. Fu, T. J. Shin, H. S. Shin, S. T. Pantelides, W. Zhou and K. P. Loh, *J. Am. Chem. Soc.*, 2017, **139**, 9392–9400.
- 53 M. Mahjouri-Samani, R. Gresback, M. Tian, K. Wang, A. A. Puzosky, C. M. Rouleau, G. Eres, I. N. Ivanov, K. Xiao, M. A. McGuire, G. Duscher and D. B. Geohegan, *Adv. Funct. Mater.*, 2014, **24**, 6365–6371.
- 54 C. R. Serrao, A. M. Diamond, S.-L. Hsu, L. You, S. Gadgil, J. Clarkson, C. Carraro, R. Maboudian, C. Hu and S. Salahuddin, *Appl. Phys. Lett.*, 2015, **106**, 052101.
- 55 M. I. Serna, S. H. Yoo, S. Moreno, Y. Xi, J. P. Oviedo, H. Choi, H. N. Alshareef, M. J. Kim, M. Minary-Jolandan and M. A. Quevedo-Lopez, *ACS Nano*, 2016, **10**, 6054–6061.
- 56 Y. Gong, J. Lin, X. Wang, G. Shi, S. Lei, Z. Lin, X. Zou, G. Ye, R. Vajtai, B. I. Yakobson, H. Terrones, M. Terrones, B. K. Tay, J. Lou, S. T. Pantelides, Z. Liu, W. Zhou and P. M. Ajayan, *Nat. Mater.*, 2014, **13**, 1135–1142.
- 57 X. Duan, C. Wang, J. C. Shaw, R. Cheng, Y. Chen, H. Li, X. Wu, Y. Tang, Q. Zhang, A. Pan, J. Jiang, R. Yu, Y. Huang and X. Duan, *Nat. Nanotechnol.*, 2014, **9**, 1024–1030.
- 58 M.-Y. Li, Y. Shi, C.-C. Cheng, L.-S. Lu, Y.-C. Lin, H.-L. Tang, M.-L. Tsai, C.-W. Chu, K.-H. Wei, J.-H. He, W.-H. Chang, K. Suenaga and L.-J. Li, *Science*, 2015, **349**, 524–528.
- 59 Z. Cai, B. Liu, X. Zou and H.-M. Cheng, *Chem. Rev.*, 2018, **118**, 6091–6133.
- 60 J. Yu, X. Hu, H. Li, X. Zhou and T. Zhai, *J. Mater. Chem. C*, 2018, **6**, 4627–4640.
- 61 B. Qin, H. Ma, M. Hossain, M. Zhong, Q. Xia, B. Li and X. Duan, *Chem. Mater.*, 2020, **32**, 10321–10347.
- 62 N. Azam, Z. Ahmadi, B. Yakupoglu, S. Elafandi, M. Tian, A. Boulesbaa and M. Mahjouri-Samani, *2D Mater.*, 2019, **7**, 015014.
- 63 P. Mehta, A. Sarma, J. Ghosh, S. Pandya, S. Pandya, P. Choudhuri, J. Govindarajan, C. I. Schrittwieser and R. Schrittwieser, *Phys. Scr.*, 2010, **82**, 055402.

- 64 S. Z. Butler, S. M. Hollen, L. Cao, Y. Cui, J. A. Gupta, H. R. Gutiérrez, T. F. Heinz, S. S. Hong, J. Huang, A. F. Ismach, E. Johnston-Halperin, M. Kuno, V. V. Plashnitsa, R. D. Robinson, R. S. Ruoff, S. Salahuddin, J. Shan, L. Shi, M. G. Spencer, M. Terrones, W. Windl and J. E. Goldberger, *ACS Nano*, 2013, **7**, 2898–2926.
- 65 H. Zhang, J. Huang, Y. Wang, R. Liu, X. Huai, J. Jiang and C. Anuso, *Opt. Commun.*, 2018, **406**, 3–17.
- 66 A. Splendiani, L. Sun, Y. Zhang, T. Li, J. Kim, C.-Y. Chim, G. Galli and F. Wang, *Nano Lett.*, 2010, **10**, 1271–1275.
- 67 Z. G. Yu, B. I. Yakobson and Y.-W. Zhang, *ACS Appl. Energy Mater.*, 2018, **1**, 4115–4121.
- 68 P. Tonndorf, R. Schmidt, P. Böttger, X. Zhang, J. Börner, A. Liebig, M. Albrecht, C. Kloc, O. Gordan, D. R. T. Zahn, S. Michaelis de Vasconcellos and R. Bratschitsch, *Opt. Express*, 2013, **21**, 4908–4916.
- 69 Y. Zhang, T.-R. Chang, B. Zhou, Y.-T. Cui, H. Yan, Z. Liu, F. Schmitt, J. Lee, R. Moore, Y. Chen, H. Lin, H.-T. Jeng, S.-K. Mo, Z. Hussain, A. Bansil and Z.-X. Shen, *Nat. Nanotechnol.*, 2014, **9**, 111–115.
- 70 X. Zhang, Q.-H. Tan, J.-B. Wu, W. Shi and P.-H. Tan, *Nanoscale*, 2016, **8**, 6435–6450.
- 71 Y. Shi, H. Li and L.-J. Li, *Chem. Soc. Rev.*, 2015, **44**, 2744–2756.
- 72 R. Lv, J. A. Robinson, R. E. Schaak, D. Sun, Y. Sun, T. E. Mallouk and M. Terrones, *Acc. Chem. Res.*, 2015, **48**, 56–64.
- 73 H. F. Liu, S. L. Wong and D. Z. Chi, *Chem. Vap. Deposition*, 2015, **21**, 241–259.
- 74 L. Yang, C. Xie, J. Jin, R. N. Ali, C. Feng, P. Liu and B. Xiang, *Nanomaterials*, 2018, **8**, 463.
- 75 M. Okada, N. Okada, W.-H. Chang, T. Shimizu, T. Kubo, M. Ishihara and T. Irisawa, *Jpn. J. Appl. Phys.*, 2021, **60**, SBBH09.
- 76 S. M. Eichfeld, L. Hossain, Y.-C. Lin, A. F. Piasecki, B. Kupp, A. G. Birdwell, R. A. Burke, N. Lu, X. Peng, J. Li, A. Azcatl, S. McDonnell, R. M. Wallace, M. J. Kim, T. S. Mayer, J. M. Redwing and J. A. Robinson, *ACS Nano*, 2015, **9**, 2080–2087.
- 77 W. Choi, N. Choudhary, G. H. Han, J. Park, D. Akinwande and Y. H. Lee, *Mater. Today*, 2017, **20**, 116–130.
- 78 N. Briggs, S. Subramanian, Z. Lin, X. Li, X. Zhang, K. Zhang, K. Xiao, D. Geohagan, R. Wallace and L.-Q. Chen, *2D Mater.*, 2019, **6**, 022001.
- 79 A. Roy, H. C. P. Movva, B. Satpati, K. Kim, R. Dey, A. Rai, T. Pramanik, S. Guchhait, E. Tutuc and S. K. Banerjee, *ACS Appl. Mater. Interfaces*, 2016, **8**, 7396–7402.
- 80 R. Yue, Y. Nie, L. A. Walsh, R. Addou, C. Liang, N. Lu, A. T. Barton, H. Zhu, Z. Che and D. Barrera, *2D Mater.*, 2017, **4**, 045019.
- 81 M. Hilse, K. Wang and R. Engel-Herbert, *2D Mater.*, 2020, **7**, 045013.
- 82 L. Zhang, T. Yang, M. F. Sahdan, Arramel, W. Xu, K. Xing, Y. P. Feng, W. Zhang, Z. Wang and A. T. S. Wee, *Adv. Electron. Mater.*, 2021, **7**, 2100559.
- 83 S. Seo, I. Oh, J.-C. Park, J. Lee, Y. Jung, H. Choi, J. Ryu and S. Lee, *ACS Appl. Nano Mater.*, 2021, **4**, 12017–12023.
- 84 I. P. Herman, *Chem. Rev.*, 1989, **89**, 1323–1357.
- 85 Y. v. d. Burgt, *J. Laser Appl.*, 2014, **26**, 032001.
- 86 J. Park, S. Jeong, M. Jeong, S. Lim, I. Lee and Y. Lee, *Nanotechnology*, 2009, **20**, 185604.
- 87 J. B. Park, S. H. Jeong and M. S. Jeong, *Appl. Surf. Sci.*, 2010, **257**, 641–649.
- 88 J. B. Park, W. Xiong, Y. Gao, M. Qian, Z. Q. Xie, M. Mitchell, Y. S. Zhou, G. H. Han, L. Jiang and Y. F. Lu, *Appl. Phys. Lett.*, 2011, **98**, 123109.
- 89 J. W. Um, S.-Y. Kim, B. H. Lee, J. B. Park and S. Jeong, *Carbon*, 2020, **169**, 163–171.
- 90 C.-T. Toh, H. Zhang, J. Lin, A. S. Mayorov, Y.-P. Wang, C. M. Orofeo, D. B. Ferry, H. Andersen, N. Kakenov, Z. Guo, I. H. Abidi, H. Sims, K. Suenaga, S. T. Pantelides and B. Özyilmaz, *Nature*, 2020, **577**, 199–203.
- 91 W.-J. Joo, J.-H. Lee, Y. Jang, S.-G. Kang, Y.-N. Kwon, J. Chung, S. Lee, C. Kim, T.-H. Kim and C.-W. Yang, *Sci. Adv.*, 2017, **3**, e1601821.
- 92 L. S. Fan, Y. Zhou, M. Wang, Y. Gao, L. Liu, J. Silvain and Y. Lu, *Laser Phys. Lett.*, 2014, **11**, 076002.
- 93 L. Constantin, L. Fan, C. Azina, K. Keramatnejad, J.-F. Silvain and Y. F. Lu, *Cryst. Growth Des.*, 2018, **18**, 2458–2466.
- 94 R. S. Yalamanchi and K. S. Harshavardhan, *J. Appl. Phys.*, 1990, **68**, 5941–5943.
- 95 K. Komaki, M. Yanagisawa and I. Y. Hirose, *Jpn. J. Appl. Phys.*, 1993, **32**, 1814.
- 96 J. A. Miller and C. F. Melius, *Combust. Flame*, 1992, **91**, 21–39.
- 97 P. C. Redfern, D. A. Horner, L. A. Curtiss and D. M. Gruen, *J. Phys. Chem.*, 1996, **100**, 11654–11663.
- 98 D. M. Gruen, P. C. Redfern, D. A. Horner, P. Zapol and L. A. Curtiss, *J. Phys. Chem. B*, 1999, **103**, 5459–5467.
- 99 M. Irion and K. Kompa, *Appl. Phys. B: Photophys. Laser Chem.*, 1982, **27**, 183–186.
- 100 B. Balko, J. Zhang and Y. T. Lee, *J. Chem. Phys.*, 1991, **94**, 7958–7966.
- 101 E. F. Cromwell, A. Stolow, M. J. Vrakking and Y. T. Lee, *J. Chem. Phys.*, 1992, **97**, 4029–4040.
- 102 T. Kovács, M. A. Blitz and P. W. Seakins, *J. Phys. Chem. A*, 2010, **114**, 4735–4741.
- 103 H. Liu and D. S. Dandy, *Diamond chemical vapor deposition: nucleation and early growth stages*, Elsevier, 1996.
- 104 O. Conde and A. J. Silvestre, *Appl. Phys. A*, 2004, **79**, 489–497.
- 105 J. Olander, L. M. Ottosson, P. Heszler, J. O. Carlsson and K. M. Larsson, *Chem. Vap. Deposition*, 2005, **11**, 330–337.
- 106 B. Sharma and A. Sharma, *Appl. Surf. Sci.*, 2021, **567**, 150724.
- 107 H. Rabiee Golgir, D. W. Li, K. Keramatnejad, Q. M. Zou, J. Xiao, F. Wang, L. Jiang, J.-F. Silvain and Y. F. Lu, *ACS Appl. Mater. Interfaces*, 2017, **9**, 21539–21547.
- 108 M. D. Dange, J. Y. Lee and K. Sooriakumar, *Microelectron. J.*, 1991, **22**, 19–26.

- 109 K. S. Kim, N. Sirse, K. H. Kim, A. R. Ellingboe, K. N. Kim and G. Y. Yeom, *J. Phys. D: Appl. Phys.*, 2016, **49**, 395201.
- 110 K. S. Kim, K. H. Kim, Y. J. Ji, J. W. Park, J. H. Shin, A. R. Ellingboe and G. Y. Yeom, *Sci. Rep.*, 2017, **7**, 13585.
- 111 P. Y. Gangavarapu, A. M. R. Sharma and A. Naik, *Semicond. Sci. Technol.*, 2019, **34**, 065018.
- 112 W. Hobson, F. Ren, U. Mohideen, R. Slusher, M. Lamont Schnoes and S. Pearton, *J. Vac. Sci. Technol., A*, 1995, **13**, 642–645.
- 113 J. Ubrig, S. Martin, S. Cros and J. Bouree, *J. Phys.: Conf. Ser.*, 2008, **100**, 082030.
- 114 M. Sugo, N. Uchida, A. Yamamoto, T. Nishioka and M. Yamaguchi, *J. Appl. Phys.*, 1989, **65**, 591–595.
- 115 A. Tarraf, J. Daleiden, S. Irmer, D. Prasai and H. Hillmer, *J. Micromech. Microeng.*, 2003, **14**, 317.
- 116 N. Gupta, A. Pandey, S. R. K. Vanjari and S. Dutta, *Microsyst. Technol.*, 2019, **25**, 3959–3967.
- 117 Y. J. Ji, K. S. Kim, K. H. Kim, J. Y. Byun and G. Y. Yeom, *Appl. Sci. Converg. Technol.*, 2019, **28**, 142–147.
- 118 Y. J. Ji, K. S. Kim, K. H. Kim, A. R. Ellingboe and G. Y. Yeom, *Appl. Surf. Sci.*, 2020, **506**, 144904.
- 119 K. An, H.-N. Lee, K.-H. Cho, Y. J. Han and K.-T. Kang, *Org. Electron.*, 2021, **91**, 106078.
- 120 K. An, H.-N. Lee, K. H. Cho, S.-W. Lee, D. J. Hwang and K.-T. Kang, *Micromachines*, 2020, **11**, 88.
- 121 K. H. Kim, K. S. Kim, Y. J. Ji, J. E. Kang and G. Y. Yeom, *Appl. Surf. Sci.*, 2021, **541**, 148313.
- 122 M. J. Helix, K. V. Vaidyanathan, B. G. Streetman, H. B. Dietrich and P. K. Chatterjee, *Thin Solid Films*, 1978, **55**, 143–148.
- 123 Y. He and J. Kanicki, *Appl. Phys. Lett.*, 2000, **76**, 661–663.
- 124 W. Huang, X. Wang, M. Sheng, L. Xu, F. Stubhan, L. Luo, T. Feng, X. Wang, F. Zhang and S. Zou, *Mater. Sci. Eng., B*, 2003, **98**, 248–254.
- 125 S. F. Chen, Y. Tian, J. Peng, H. Zhang, X. J. Feng, H. Zhang, X. Xu, L. Li and J. Gao, *J. Mater. Chem. C*, 2015, **3**, 6822–6830.
- 126 D. Yin, J. Feng, R. Ma, Y.-F. Liu, Y.-L. Zhang, X.-L. Zhang, Y.-G. Bi, Q.-D. Chen and H.-B. Sun, *Nat. Commun.*, 2016, **7**, 11573.
- 127 Y. Jiang, Y.-Y. Liu, X. Liu, H. Lin, K. Gao, W.-Y. Lai and W. Huang, *Chem. Soc. Rev.*, 2020, **49**, 5885–5944.